Spatio-Temporal Characteristics of UHI in Coastal Urban Area and its Impact on Land Unit: A Case Study in the Southeast Sulawesi Province, Indonesia

Nurgiantoro[1*] Hadini, L. O.,[1] Jahidin,[2] Alfat, S.,[3] Zulfikar,[4] Uslinawaty, Z.,[5] Mokui, H. T.[6] and Aris, A.[7]

[1]Department of Geography, Universitas Halu Oleo, Kendari, 93232, Southeast Sulawesi, Indonesia
E-mail: nurgiantoro@uho.ac.id,* laodehadini@uho.ac.id

[2]Department of Geophysical Engineering, Universitas Halu Oleo, Kendari, 93232, Southeast Sulawesi, Indonesia, E-mail: jahidin_geofisika@uho.ac.id

[3]Department of Physics Education, Universitas Halu Oleo, Kendari, 93232, Southeast Sulawesi, Indonesia
E-mail: sayahdin.alfat@yahoo.com

[4]Department of Soil Science, Universitas Halu Oleo, Kendari, 93232, Southeast Sulawesi, Indonesia
E-mail: zulfikar@uho.ac.id

[5]Department of Forestry, Universitas Halu Oleo, Kendari, 93232, Southeast Sulawesi, Indonesia
E-mail: zakiahuslinawati@gmail.com

[6]Department of Electrical Engineering, Universitas Halu Oleo, Kendari, 93232, Southeast Sulawesi, Indonesia
E-mail: hasmina.mokui@uho.ac.id

[7]Department of Urban and Regional Planning, Universitas Halu Oleo, Kendari, 93232, Southeast Sulawesi, Indonesia, E-mail: armayanti.aris@uho.ac.id

**Corresponding Author*

DOI: https://doi.org/10.52939/ijg.v21i2.3945

Abstract

The dynamics of urban heat island (UHI) in urban thermal environments will be more complex and crucial along with the region rapid growth, coupled with increasingly an unforeseen global temperature condition. This study aims to observe the characteristics of UHI and its effects on land units in coastal cities in Southeast Sulawesi province from 2019 to 2023. Landsat 8/9 imagery is used for Land Surface Temperature (LST) retrieval. Urban Landscape Composition (ULC) is developed based on the spectral index method through VrNIR-BI, NDVI and MNDWI. Land units are developed using overlay techniques from four input data including ULC, terrain slope, soil type and geological formation. The results of the study reveal that LST variations significantly affect UHI formation throughout the study area. Surface temperatures in both regions continued to increase throughout 2021-2023, is getting warmer in 2023 between August and November. Meanwhile, the ULC conditions in both regions experienced major transformations, especially in the areas of impervious surface and green space. Nevertheless, over 70% of the total area in both regions is covered by vegetation. Spatially, the UHI changes in Kendari city tends to moved towards the western region and are more massive to the southern region. Meanwhile, the UHI area in Baubau city is still relatively in the downtown area, but several areas in the northern region of Baubau are beginning to show substantial UHI concentration. Global warming that occurred in 2023 further worsened the UHI in both regions. The UHI area is typically affect more land units categorized as impervious surface with relatively flat terrain slopes and hapludalfs soil types. This study emphasizes the importance of studying the dynamics of microclimate in urban thermal environments in the disaster mitigation efforts, providing valuable insights for regional development planning strategies to create environmentally friendly, resilient and sustainable cities

Keywords: Coastal Cities, Land Surface Temperature, Land Units, Urban Heat Island, Urban Landscape

1. Introduction

Rapid urbanization in the 21st century has created increasingly massive urbanization activities in all sectors of human life. These activities occur in many regions around the world and most of them are found in medium-sized cities that are starting to become large cities [1].

The rapid development of regional infrastructure in various sectors in urban areas such as housing and residential areas, transportation, and various public service areas has caused a major transformation in the composition and structure of land use in urban areas [2] creating a widely fragmented impervious surface area [3], and linearly causing various urban environmental problems, especially the increase in Land Surface Temperature (LST) globally [4] which can exacerbate microclimate conditions in urban areas.

The complexity of microclimate problems in urban areas is generally known as the Urban Heat Island (UHI), which refers to changes in the warmer thermal climate in urban areas than the surrounding areas, particularly at night [5]. In some cases, the temperature difference between urban areas and surrounding areas ranges from 0.5° – 4℃ during the day and 1° – 2.5℃ at night [6]. Even at its maximum condition it can reach 10° – 15℃ [7]. Spatially, the UHI area is generally influenced by the concentration of LST, an increase in the UHI area will be in line with the increase in the average LST in urban areas. The main findings of the global average annual temperature predicted to reach 1.4° – 5.7℃ in 2050-2100 [8] and [9] are predicted to further exacerbate the UHI area in urban environments. In addition, other factors such as urban geometry related to building density [10] and anthropogenic heat releases related to anthropogenic heat flux including heat generated by internal combustion vehicles, heat released by industrial processes, heat generated by electricity and/or gas consumption, and the metabolic heat produced by humans [11] also affect the increase in UHI. Even now the influence of the slope of the terrain, soil type and geological formation in urban areas is becoming a new study in UHI cases [12] and [13].

The UHI effect has negative impacts on the urban environment, including changing the climate system, threatening biodiversity, affecting ecosystem productivity and losing carbon storage [14]. Even so, UHI has favorable effects in certain regions, especially in areas with very cold winters [15]. Currently, studies related to the UHI effect are increasingly interesting to study along with the rapid development of remote sensing technology such as Landsat technology. The Operational Land Imager (OLI) data and thermal infrared sensor (TIRS) data onboard Landsat 8/9 are also provided for free download in both data collection 1 and data collection 2. Then, the operation of Landsat 9 in conjunction with Landsat 8 has made the Landsat earth observation period 8 days shorter than the previous 16 days. This certainly benefits researchers, especially in areas near the equator line who often have difficulty in selecting data free from cloud cover, such as the Indonesian region.

Indonesia is an archipelago in Southeast Asia right on the equator line with full sunlight throughout the year. As one of the largest archipelagic countries in the world, the physical development of urban areas in Indonesia makes extensive use of coastal areas. This will certainly have an impact on the quality of the urban thermal environment because this environment is significantly influenced by changes in land use land cover [16]. Meanwhile, the increasing human population causes significant environmental pressure, especially for urban areas [17]. Citing population data from the Directorate General of Population and Civil Registration of the Ministry of Home Affairs, Indonesia's population will reach 280 million inhabitants 2023 and more than 55 percent live in urban areas. Indonesia currently has 98 autonomous cities, 54 percent of which are coastal cities, including the cities of Kendari and Baubau in Southeast Sulawesi province. Kendari city is the first city to be formed autonomously in 1995, then Baubau city in 2001.

As a coastal city and the capital of Southeast Sulawesi, Kendari city has different landform characteristics compared to Baubau city. Topographically, Kendari city is dominated by plains and some hills, while Baubau city generally has mountainous, undulating and hilly surfaces. As is known, different landform conditions play an important role in the formation of UHI [18] where urban infrastructure development will be accelerated on land forms with flat topography. In addition, along with expansion of the city, infrastructure projects such as ports and airports, roads and bridges, housing and high-rise buildings, and other public facilities are now being carried out massively in the Kendari and Baubau Cities. The expansion of this infrastructure will certainly change land units, especially on natural land cover which has a negative impact on the urban thermal environment [16] and affects the balance of the microclimate in both cities which are expected is getting warmer in the future.

Previous studies related to UHI and its effects have been widely studied in various cities in the world, including in Indonesia. The results of these studies are mostly based on remote sensing data, especially using Landsat imagery, but the spatio-temporal data studied is still limited and the observation years are not sequential. For the case of UHI in Indonesia, more studies have been found in major cities in the western region of Indonesia, particularly on Java Island.

While cities in the central Indonesia region located on the Island of Sulawesi which are generally coastal cities, especially in Southeast Sulawesi province are remains limited. Meanwhile, studies related to UHI and its effects in coastal cities on land units have not been widely found. That is exactly what will be implemented in our research. In this study, Landsat imagery data ranged from 2019 to 2023 are free from the effects of cloud cover and its shadow was used to study the characteristics of UHI and observe its effects on each land unit, developed simultaneously from four parameters including urban landscape composition, terrain slope, soil type, and geological formation by retrieving a case of coastal cities located in the region of Southeast Sulawesi, namely Kendari and Baubau cities. The purpose of this study is to observe the characteristics of UHI and its effects on land units in coastal cities in Southeast Sulawesi province from 2019 to 2023. This research objective is a spatial and temporal study related to the characteristics of UHI and observations of the effects of UHI on land units in coastal city areas.

2. Study Area

The study site in this research are the coastal cities of Southeast Sulawesi province. Southeast Sulawesi is one of the provinces in Indonesia located on the island of Sulawesi. Administratively, consisting of 15 districts and 2 municipalities, including Kendari and Baubau cities and has two seasons of the dry season and the rainy season. Kendari city is located on the southeast coast of Sulawesi Island at coordinates of 3°54′40″ – 4°5′05″S and 122°26′33″ – 122°39′14″E. It has an area of 268.20 Km² and a total population of 364,220 inhabitants 2023. Meanwhile, Baubau city is located on the southern coast of the Island of Buton at coordinates of 5°18′30″ – 5°32′18″S and 122°33′22″ – 122°46′12″E. It has an area of 289.60 Km² and a total population of 166,150 inhabitants 2023. Based on data from the Agency for Meteorology Climatology and Geophysics (BMKG) weather stations through the Kendari Maritime Meteorological Station and the Betoambari Meteorological Station, the average monthly air temperatures in both regions of 27.62℃ and 27.55℃ respectively in 2023. The research areas are as shown in Figure 1.

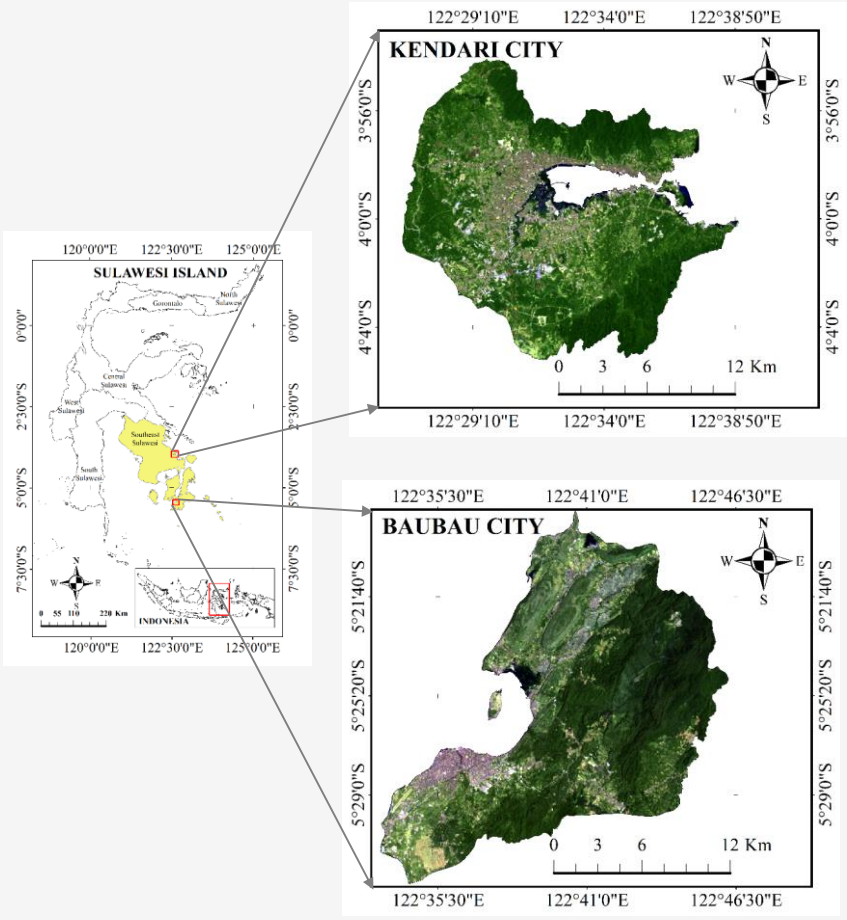

Figure 1: Southeast Sulawesi province, Indonesia

Table 1: Primary data collection

Path/row:112/63		Path/row:112/64	
Landsat scene ID	**Acquisition date**	**Landsat scene ID**	**Acquisition date**
LC81120632019088LGN00	March 29, 2019	LC81120642019264LGN00	September 21, 2019
LC81120632020107LGN00	August 22, 2020	LC81120642020235LGN00	August 22, 2020
LC81120632021045LGN00	February 14, 2021	LC81120642021077LGN00	March 18, 2021
LC91120632022216LGN01	August 4, 2022	LC91120642022232LGN02	August 20, 2022
LC91120632023299LGN00	October 26, 2023	LC91120642023315LGN00	November 11, 2023

3. Material and Methods

3.1 Data Description

3.1.1 Primary data

This research uses Landsat 8/9 imagery as primary data to calculate the UHI area. We collected OLI data from 2019 to 2023 on path/row: 112/063 and 112/064 based on level 2 and TIRS data based on level 1 data processing. The data acquisition dates present in Table 1. In addition, we also used Quality Assessment (QA_PIXEL) band data to optimize the pixel values [19] of the Landsat data that we processed. This decision aims to eliminate the effects of cloud cover and its shadow on the LST retrieval process, because the study area is near the equator line with massive cloud formation throughout the year. The primary data in this study was collected through from the official Landsat data provider website at https://earthexplorer.usgs.gov.

3.1.2 Secondary data

The secondary data format in this research is raster and vector data used in land unit analysis. The raster data is the Digital Elevation Model Nasional (DEMNAS) data obtained from the Geospatial Information Agency (BIG) web portal via https://tanahair.indonesia.go.id/demnas. While the vector data includes administrative boundary data, soil types and geological formation data for the Southeast Sulawesi region.

3.2 Data Processing

3.2.1 Removing cloud and cloud shadow

Cloud cover and its shadow will affect the LST value if not eliminated in Landsat image processing. Therefore, in this study, the pixel value of the cloud and its shadow was set to 0 and the others are set to 1 using the QA_PIXEL band. Technically, the pixel value in the band is set by scripting on the raster calculator platform of ArcGIS tools. The assigns scripted by Con (QA_PIXEL >= cloud pixel value,0,1), where the cloud pixel value is obtained from the QA_PIXEL band. The pixel value of 22080 with the description of mid confidence cloud [19], that is exactly what will be assigned for the process of removing cloud and cloud shadow in the study area. The raster output from this processing will be calculated with the OLI and TIRS bands and each raster produced from this calculation is used in the subsequent processing.

3.2.2 Land Surface Temperature (LST) retrieval

Land Surface Temperature is the main parameter in UHI analysis. The derivation of LST from Landsat imagery mainly uses the thermal band at wavelengths of 10.40 – 12.50 µm and 10.60 – 11.19 µm on Landsat 7 and 8/9, respectively. However, to maximize LST retrieval from Landsat data, several conversion processes for the raw thermal band are absolutely necessary and important. These processes include converting the digital number value of the thermal band into spectral radiance, then the raster results from the conversion are converted into at-satellite brightness temperature. The conversion formulas are respectively based on Equation 1 and Equation 2 [20] and [21] as follows.

$$L_\lambda = M_L Q_{cal} + A_L \qquad \text{Equation 1}$$

Where L_λ is the spectral radiance at the sensor's aperture in $Wm^{-2}sr^{-1}\mu m^{-1}$, M_L is band specific multiplicative rescaling factor or in the metadata referred to as RADIANCE_MULT_BAND_10, A_L is band specific additive rescaling factor or in the metadata referred to as RADIANCE_ADD_BAND _10, and Q_{cal} is quantized and calibrated standard product pixel values.

$$T_B = \frac{K_2}{\ln\left(\frac{K_1}{L_\lambda}+1\right)} \qquad \text{Equation 2}$$

Where T_B is the brightness temperature in Kelvin units, K_1 and K_2 are band specific thermal conversion constant or in the metadata is referred to as K1_CONSTANT_BAND_10 and K2_CONSTA NT_BAND_10.

The next step of the brightness temperature value that has been referenced into Kelvin units is the basis for calculating LST.

However, in this research area, we mapped LST in Celsius units, developed based on TIRS band 10 onboard Landsat 8/9 and some constant assigns such as Boltzmann Constant and Planck Constant, also the influence of Land Surface Emissivity (LSE) according to the nature of land cover by reference to the emissivity classification developed by Sobrino et al [22] and [23]. The LST retrieval were computed according to Equation 3 [20].

$$LST = \frac{T_B}{1+\left(\lambda \frac{T_B}{\rho}\right)\ln \varepsilon} - 273.15$$

Equation 3

Where λ is the central band wavelength of emitted radiance, λ = 10.8 μm for TIRS band 10 [4] and [24] onboard L8/L9, $\rho = h \times c/\sigma$ (1.438×10^{-2} mK), σ is the Boltzmann constant (1.38×10^{-23} J/K), h is Planck's constant (6.626×10^{-34} Js), c is the velocity of light (2.998×10^{8} ms^{-1}) and ε is the LSE according to Equation 4 [22] and [23].

$$\varepsilon = mP_v + n$$

Equation 4

Where:

$$P_v = \left(\frac{NDVI - NDVI_{\min}}{NDVI_{\max} - NDVI'_{\min}}\right)^2$$

Equation 5

and,

$$NDVI = \frac{\rho_{NIR} - \rho_{Red}}{\rho_{NIR} + \rho_{Red}}$$

Equation 6

Where, m and n are the soil emissivity and vegetation emissivity, respectively (m = 0.004 and n = 0.986). The P_v is the vegetation proportion and was derived using Equation 5 [4] and [24]. $NDVI_{\min}$ is minimum value of the NDVI, and the $NDVI_{\max}$ is maximum value of the NDVI. The NDVI was derived using Equation 6 [25][26] and [27]. ρ_{Red} and ρ_{NIR} are the spectral reflectance bands 4 and 5 respectively in the OLI data.

3.2.3 Urban Heat Island (UHI) retrieval

Urban Heat Island is a microclimate phenomenon which refers to changes in the warmer thermal climate in urban areas than the surrounding areas [5]. The meaning of surrounding area is basically synonymous with urban peripheral area or rural area. Based on satellite imagery, the distribution of UHI and non-UHI areas can be mapped based on the concentration of surface temperature typically processed by LST-based threshold method [28] and [7]. In this research study, we applied this method to denote the spatial distribution of UHI area of the study site. Technically, the area of UHI will be calculated based on the following Equation 7 [28] and [7].

$$LST > \mu + 0.5SD$$

Equation 7

Where, μ and SD are the mean and standard deviation of temperatures in study area, respectively.

3.2.4 Urban Landscape Composition (ULC) retrieval

In this study, the Urban Landscape Composition (ULC) of study area was separated into three categories of the green space (GS), impervious surface (IS) and water body (Wr), developed based on the spectral index methods. The categories of GS, IS and Wr are determined by the normalized difference vegetation index (NDVI), the visible red-based built-up indices (VrNIR-BI) and the modified normalized difference water index (MNDWI) respectively, calculated based on Equations 6, 8 [4] and 9 [29]. The results of processing from several indexes are classified into two with a range of values determined based on the natural conditions of the study area. As the end of this stage, raster to vector (*R* to *V*) conversion is carried out for the process of merging and eliminating field data. Polygon vectors that indicate the ULC category will be merged and other vectors will be eliminated.

$$VrNIR - BI = \frac{\rho_{Red} - \rho_{NIR}}{\rho_{Red} - \rho_{NIR}}$$

Equation 8

$$MNDWI = \frac{\rho_{Green} - \rho_{SWIR1}}{\rho_{Green} + \rho_{SWIR1}}$$

Equation 9

Where ρ_{Green}, ρ_{Red}, ρ_{NIR} and ρ_{SWIR1} refer to the surface reflectance values of bands 3, 4, 5, and 6 of the Landsat 8/9 imagery, respectively.

3.2.5 Land unit mapping

In this stage of the study, we use overlay analysis to determine land units in the study area. The input parameters analyzed include ULC, terrain slope, soil type, and geological formation. The ULC and slope parameters are obtained from the results of processing landscape composition and DEMNAS data with descriptions and classifications as shown in Table 2.

While the soil type and geological formation parameters are secondary data obtained from the relevant Government Agency. Geographically, each of the parameters mentioned above is presented in Figure 2. The UHI area in the last year's data is used to show how much UHI is formed in each land unit.

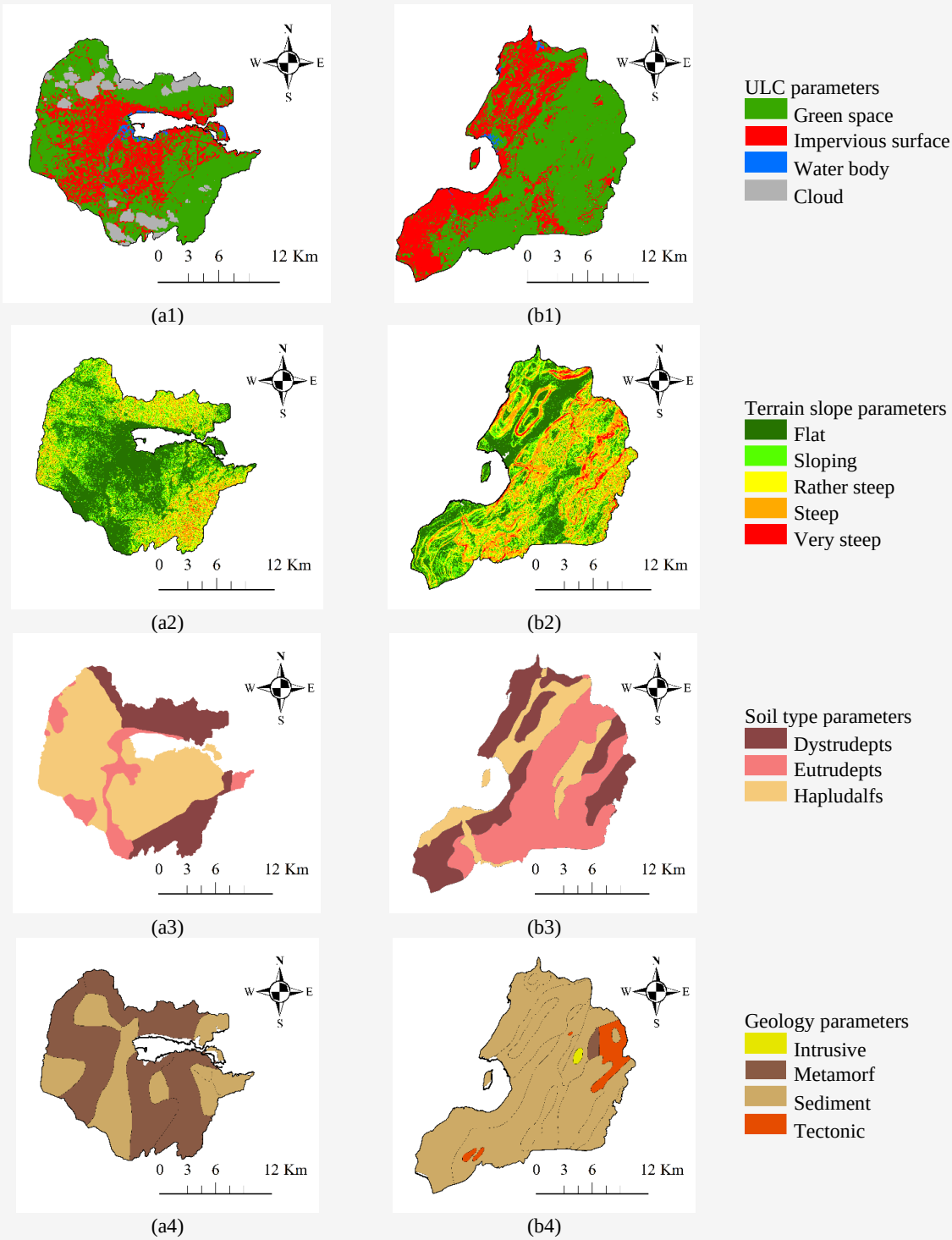

Figure 2: Parameters visualized on land units:
(a1) to (a4) are the parameters of ULC, terrain slope, soil type and geology in the Kendari region respectively;
(b1) to (b5) are the parameters of ULC, terrain slope, soil type and geology in the Baubau region respectively

Table 2: Land unit parameters

Parameters	Description	Classify	Code	Availability of parameters	
				Kendari city	Baubau city
ULC	Green space	Green space	GS	A	A
	Impervious surface	Impervious surface	IS	A	A
	Water body	Water body	Wr	A	A
Terrain slope	Flat	0 – 8%	Fl	A	A
	Sloping	8 – 15%	Sl	A	A
	Rather steep	15 – 25%	Rs	A	A
	Steep	25 – 45%	St	A	A
	Very steep	> 45%	Vs	A	A
Soil type	Dystrudepts	Dystrudepts	Dys	A	A
	Eutrudepts	Eutrudepts	Eut	A	A
	Hapludalfs	Hapludalfs	Hap	A	A
Geology	Intrusive	Intrusive	Geo1	N/A	A
	Metamorf	Metamorf	Geo2	A	A
	Sediment	Sediment	Geo3	A	A
	Tectonic	Tectonic	Geo4	N/A	A

Table 3: Average LST change

Year	Kendari city		Baubau city	
	LST value (℃)	LST change (℃)	LST value (℃)	LST change (℃)
2019	23.1		28.0	
2020	24.0	+0.9	25.5	-2.5
2021	22.3	-1.7	23.8	-1.7
2022	25.3	+3.0	25.0	+1.2
2023	32.3	+7.0	31.7	+6.7

4. Results and Discussion

4.1 Average Land Surface Temperature Changes

Based on LST calculation, LST distribution in Kendari and Baubau cities are highlighted in blue, yellow, orange, red and brown color gradations. Some classifications of LST values that have been divided are LST Value > 20° to 25℃, LST > 25° to 30℃, LST > 30° to 35℃ and LST > 35° to 40℃ which are then shown in blue to yellow, yellow to orange, orange to red, and red to brown, respectively, as presented in Figure 3. Further, changes in the average LST value based on Landsat 8/9 image processing in both cities and their differences are shown in Table 3 and Table 4.

Based on Figure 3, the distribution of LST in Kendari and Baubau cities shows that the concentration is higher in the city center area and gradually decreases in the surrounding areas. Changes in LST in both cities experienced increases and decreases during the period 2019-2023. Based on Table 3, in general, the average LST of Kendari city calculated based on Landsat imagery from 2020-2023 shows a value that is relatively close to the LST in the Baubau city area. However, the average LST in 2019 showed different results in the two areas. The calculation of the difference in LST values between the two regions in 2019 or ΔLST reached 4.9℃ higher than other years which ranged from 0.3℃ to 1.5℃ as shown in Table 4. The difference in Landsat image acquisition in 2019 which was used as the basis for calculating LST in the two cities are the reason why this could happen, where in the case of Kendari city, LST was calculated based on data from March 2019, five months apart from Baubau city which was calculated in September. The massive cloud cover throughout 2019 was an obstacle in the Landsat image collection process, especially for the Kendari city area. In addition, seasonal variations in a region also affect the LST analysis [27], where in Indonesia it is generally described on a seasonal scale, namely the rainy season which generally occurs in March-June and the dry season generally in August-November. Even so, the LST results during the observation period can be used as a basis for calculating the UHI area in both regions.

Based on Table 3, LST changes in the 2020-2023 period show a consistent direction in both cities. However, different results were shown in 2019-2020 where LST changes for the two cities were in opposite directions. The reasons for this difference in results have been explained in detail in the previous paragraph. Still with the same table, the LST of both cities in the 2021-2023 period continues to increase. Significant LST changes occurred in 2022-2023 where the LST change in Kendari region was +0.3℃ greater than the LST change of +6.7℃ that occurred in the Baubau region.

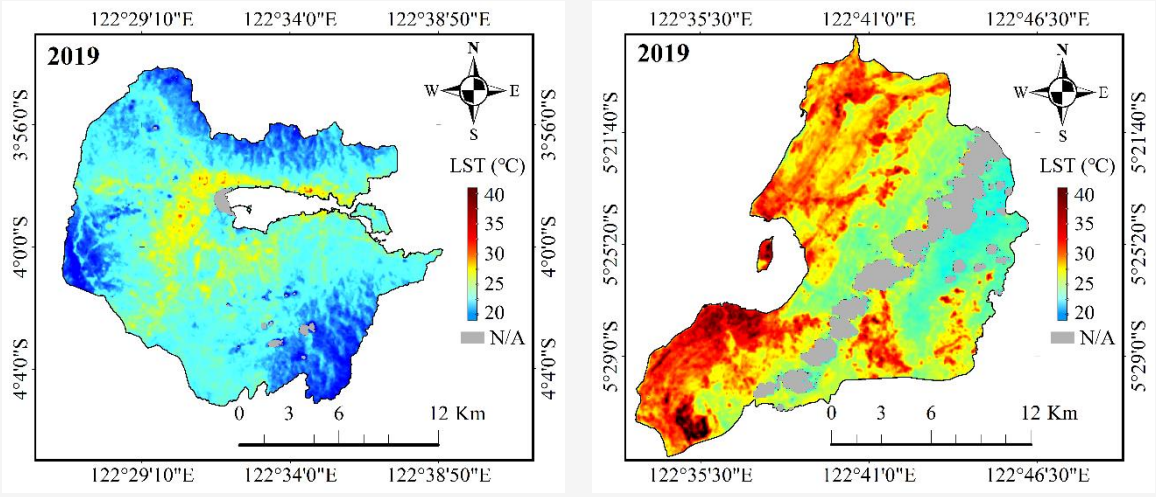

(a1) (b1)

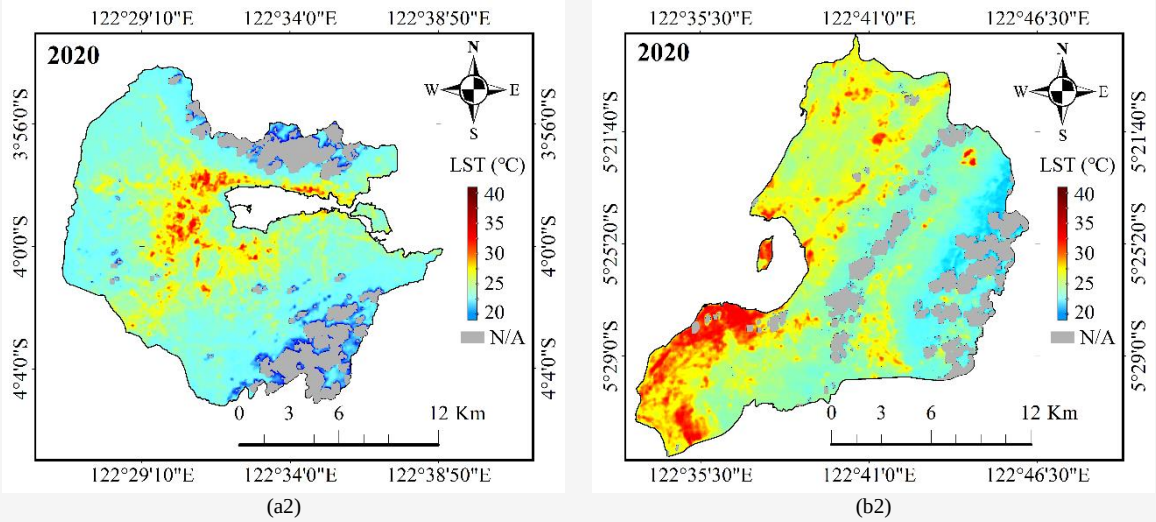

(a2) (b2)

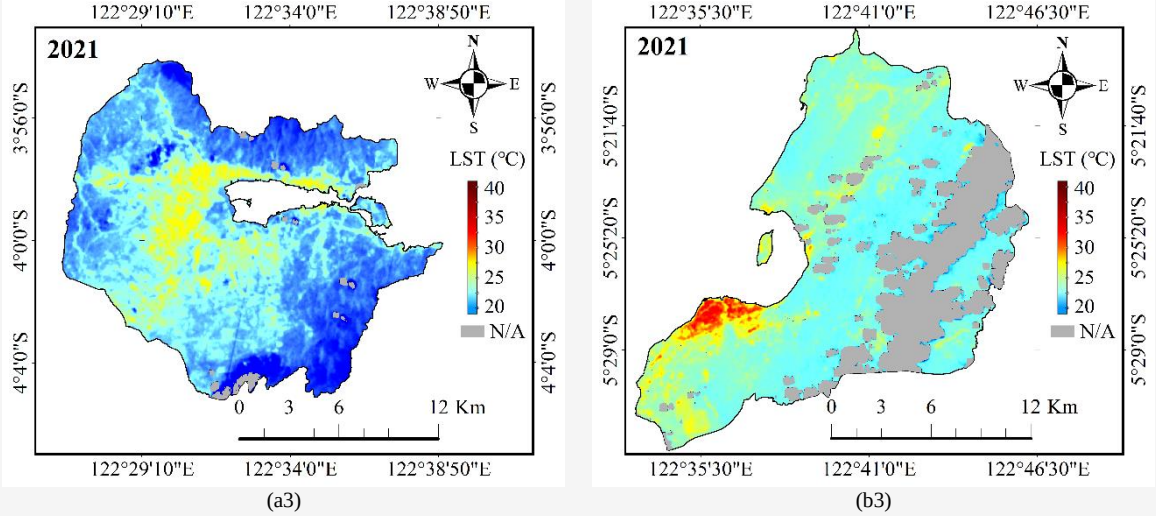

(a3) (b3)

Figure 3: LST map of study area from 2019 to 2023:
(a1) – (a5) Kendari city and (b1) – (b5) Baubau city *(Continue next page)*

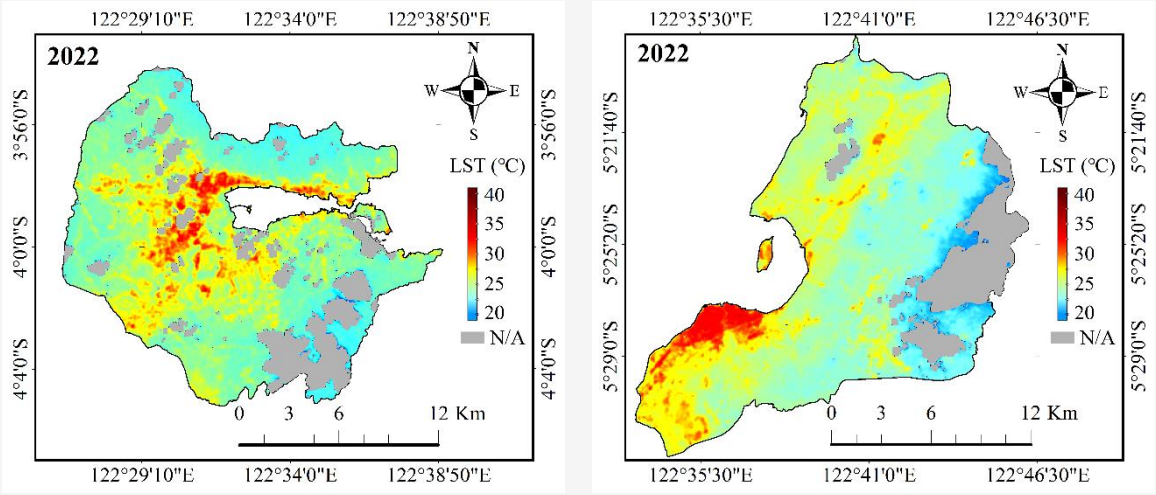

(a4) (b4)

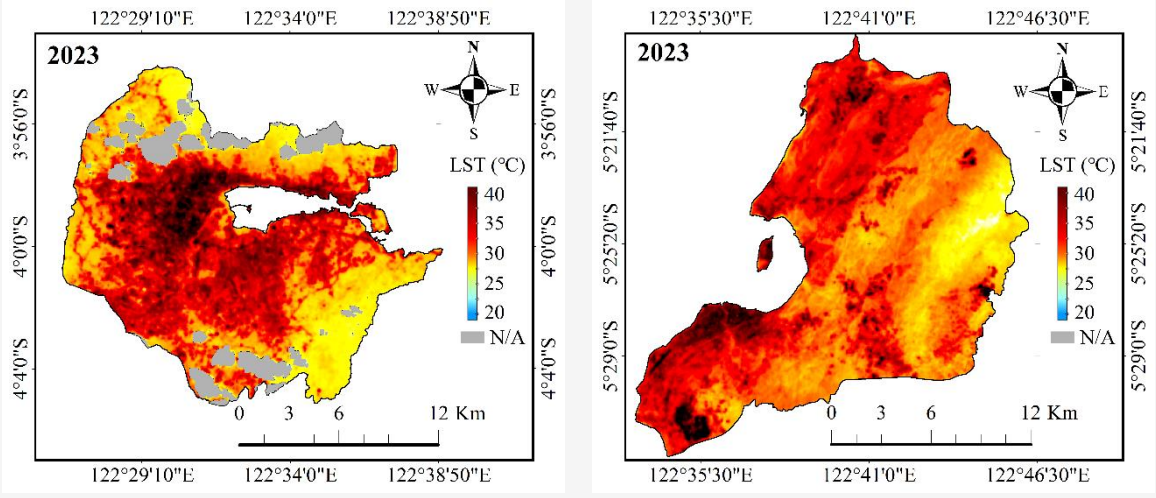

(a5) (b5)

Figure 3: LST map of study area from 2019 to 2023:
(a1) – (a5) Kendari city and (b1) – (b5) Baubau city *(Continue from previous page)*

Table 4: Average LST difference

Year	LST value (°C)						ΔLST (°C)		
	Kendari city			Baubau city					
	Max	Mean	Min	Max	Mean	Min	Max	Mean	Min
2019	29.0	23.1	19.5	37.6	28.0	20.9	8.6	4.9	1.3
2020	30.5	24.0	18.6	34.3	25.5	19.0	3.8	1.5	0.4
2021	27.7	22.3	15.1	30.9	23.8	17.1	3.2	1.5	2.0
2022	32.7	25.3	17.7	34.1	25.0	16.9	1.4	0.3	0.7
2023	41.9	32.3	23.6	43.2	31.7	26.7	1.3	0.6	3.1

Based on Table 4, 2023 was the warmest year in both cities, it has not been experienced before. This year the summer was very warm occurred in October-November, the highest LST in the two regions reached 41.9°C and 43.2°C respectively. Even the lowest LST value this year has equaled the average LST value of other years. On an urban scale, thermal variations in the urban thermal environment are normally affected by land use and land cover types [24][27] and [30], material properties [27], the ratio of green volume to built-up volume [31] and global climate conditions. Thus, the high surface temperatures that occurred in both cities in 2023 was probably influenced by the global warming event.

According to the latest The World Meteorological Organization State of the Global Climate 2023 report confirms that the year 2023 broke every single climate indicator. It was by far the warmest year on record [32]. Other sources have concluded that the many prominent events in various parts of the world such as heat waves that occurred continuously for up to 20 days longer than the previous event, then there were changes in seasons and major heat waves in several regions in Europe, Africa and Asia further confirm that 2023 was the warmest year on Earth [33]. Meanwhile, based on a report from the Climate Change Information Center - Deputy for Climatology of the Indonesian Meteorological, Climatological, and Geophysical Agency in the period October-November 2023, the Southeast Sulawesi region is still affected by moderate El Niño-Southern Oscillation (ENSO) with meteorological drought conditions on alert status [34] and [35]. This drought condition also affects the increase in LST in an area [36].

4.2 Distribution of Urban Landscape Composition and Urban Heat Island

The spatio-temporal area of UHI in our research location highlighted in red as shown in Figures 4(b1) to (b5) and 4(d1) to (d5). The UHI area map during the observation period in both cities are lined up the ULC distribution map categorized as areas of impervious surface, green space and water body as shown in Figures 4(a1) to (a5) and 4(c1) to (c5). The area of ULC categories in the study are shown in Tables 5 and 6, respectively. The area in Km² based on UHI and its percentage are shown in Table 7. In this study, the spatio-temporal UHI results are displayed together with the classification of urban landscape composition categorized as impervious surface areas, green spaces and water bodies developed through the spectral index of Landsat satellite imagery. The UHI results calculated in Kendari and Baubau cities in the 2019-2023 period show varying distributions as displayed in Figure 4 and shown in Table 7. Based on Table 7 in 2019 and 2020 the UHI area in both cities showed opposite differences, Kendari city experienced an increase in the UHI area of 1.2 Km^2 or 0.44% more than the previous year, then Baubau city experienced a decrease of 6.43 KM2 or 2.22% less in area, this happened because the dynamics of UHI were influenced by variations in LST in each region. Furthermore, in the 2021-2023 period the UHI area in both cities continued to expand.

Based on Figure 4, spatially the UHI area in Kendari city appears to be clustered, this is different from Baubau city which appears to be randomly distributed. For the case of UHI in Kendari city, the dynamics of change were initially only centered in the area around the bay which characterizes it as a coastal city, but now it has moved towards the western region and more massively to the southern region. Meanwhile, the UHI area in Baubau city is still relatively in the downtown area, but several areas in the northern region of Baubau are beginning to show substantial UHI concentration.

Table 5: Areas of ULC in the region of Kendari from 2019 to 2023

Year	IS		GS		Water body	
	Km^2	%	Km^2	%	Km^2	%
2019	58.66	21.87	206.10	76.85	3.44	1.28
2020	64.31	23.98	199.85	74.51	4.05	1.51
2021	64.23	23.95	200.51	74.76	3.46	1.29
2022	69.11	25.77	196.22	73.16	2.88	1.07
2023	95.50	35.61	169.89	63.34	2.81	1.05

Table 6: Areas of ULC in the region of Baubau from 2019 to 2023

Year	IS		GS		Water body	
	Km^2	%	Km^2	%	Km^2	%
2019	73.54	25.39	214.53	74.08	1.54	0.53
2020	64.09	22.13	223.90	77.31	1.61	0.56
2021	44.31	15.30	243.76	84.17	1.53	0.53
2022	55.77	19.26	231.88	80.07	1.96	0.68
2023	97.79	33.77	190.23	65.69	1.59	0.55

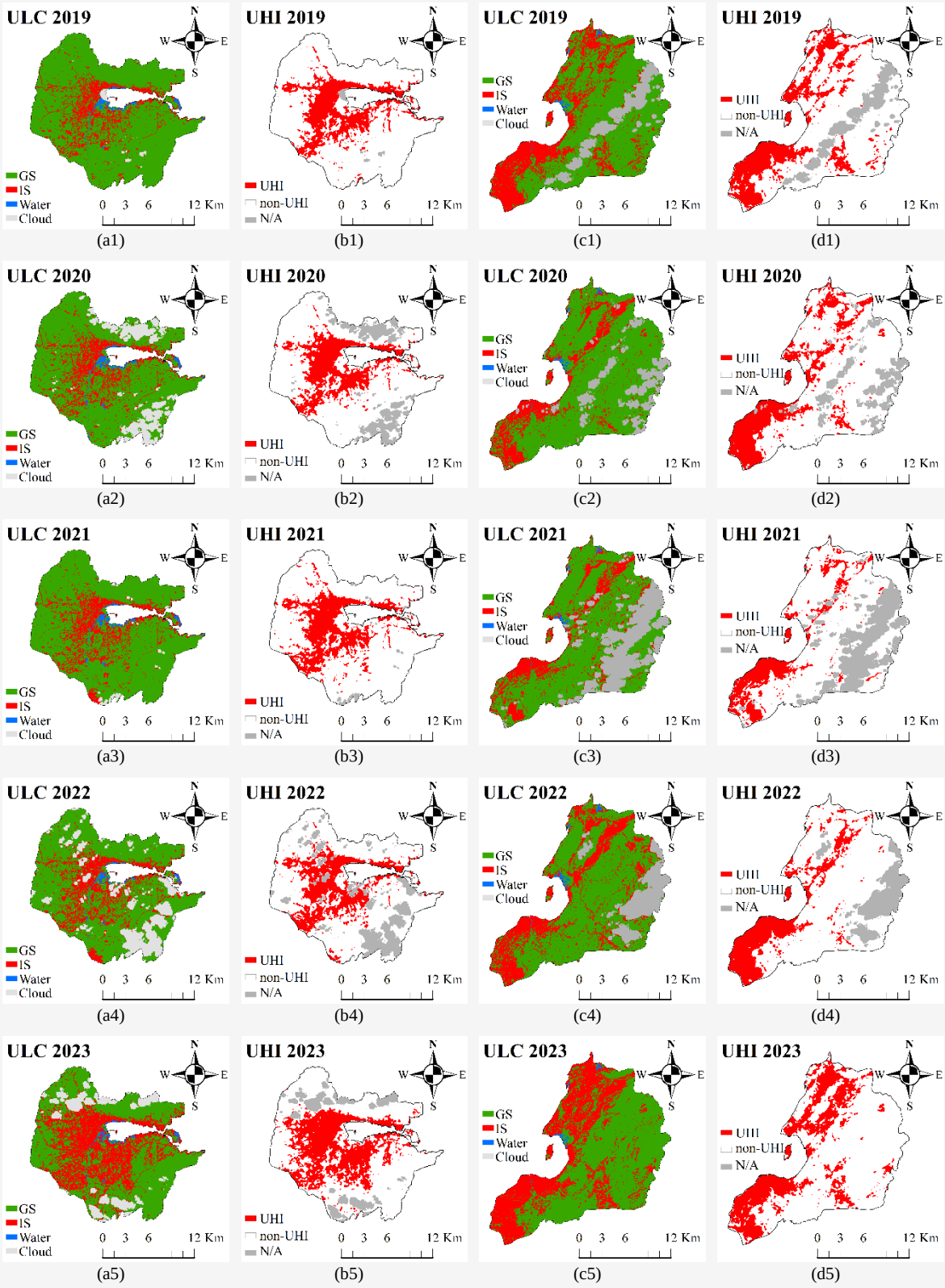

Figure 4: Map of UHI area and ULC distribution in both cities during 2019-2023: (a1) – (a5) is the ULC distribution in Kendari city; (b1) – (b5) is the UHI area in Kendari city; (c1) – (c5) is the ULC distribution in Baubau city; (d1) – (d5) is the UHI area in Baubau city

Table 7: Area in Km² based on UHI and its percentage to the study area

Year	Kendari city		Baubau city	
	UHI area (Km²)	Percentage (%)	UHI area (Km²)	Percentage (%)
2019	59.02	22.01	72.51	25.04
2020	60.22	22.45	66.08	22.82
2021	60.02	22.38	43.45	15.00
2022	65.09	24.27	57.84	19.97
2023	81.47	30.38	84.32	29.12

However, findings related to UHI in both study areas still require more detailed information, for example added the observation period to be longer and UHI analysis calculated down to the smallest areas such as sub-districts. Even so, information from the results of the expansion trend and direction of UHI movement that has been presented in the future can be used as a reference for stakeholders in both areas, especially in terms of disaster mitigation due to increasing surface temperatures. Furthermore, referring to the ULC results shown in Table 5 and Table 6, the ULC in both cities experienced varying changes during the 2019-2023 period. Spatially, changes in ULC in both regions significantly occurred in ULC categorized as impervious surface areas and green space areas, while in water bodies there was relatively no change or tended to remain the same with a percentage area of <2% for Kendari city and no more than 1% for Baubau city. The average change in the impervious surface area in Kendari and Baubau cities showed 70.36 Km² and 67.10 Km² respectively with the percentage change that occurred in Kendari city being 26.23%, which is 3.06% greater than the change that occurred in Baubau city. The reason is likely because Kendari city is the capital city of Southeast Sulawesi province so that urbanization activities such as infrastructure development in its area are more massive than Baubau city because infrastructure development always changes green landscapes into impervious surfaces. The area is an area where solar heat energy will be absorbed more than reflected [5] and [27] or an area that typically characterizes as an urban area that has a positive correlation with LST [4][29] and [26]. Land cover materials in the impervious surface area are generally dominated by low-albedo materials that are identical to concrete and asphalt [37][38] and [39] as a result, UHI will continue to be concentrated in the impervious surface area. This is in line with the findings in our research, where ULC which is categorized as an impervious surface area is the center of massive UHI formation in both regions. In fact, the dynamics of UHI changes in both cities show the same pattern as the impervious surface area, see Figure 5.

Meanwhile, the correlation results between VrNIR-BI and LST for each study area also show a positive correlation as shown in Figure 6(a2) and Figure 6(b2). However, more than 70% of the area in Kendari city and more than 75% of the area in Baubau city are green space areas or areas that have a negative correlation to LST as shown in Figure 6(a3) and Figure 6(b3). The findings of these results are certainly very useful in the future, especially in terms of monitoring and evaluation of built-up areas or in planning green belts in urban areas based on local climate zones (LCZ).

4.3 Distribution of Urban Heat Island in Various Land Units

Based on the overlay results of the land unit formation parameters, map of the distribution area of UHI on the land unit formation in the Kendari and Baubau regions are shown in Figure 7. Further, the UHI area in Km2 on various land units is shown in Table 8. The illustration of the UHI area on each land unit formation displayed in a bar graph as shown in Figure 8. Based on the results of the overlay analysis of four parameters, each of which includes urban landscape composition, terrain slope, soil type, and geological formation developed as a basis for mapping land units in both regions, of the 39 existing land units as shown in Table 8, 37 of them were formed in the region of Kendari and 35 of them were formed in the region of Baubau. Land units with the code names Is_Vs_Eut (land unit 29) and Wr_Vs_Hap (land unit 39) were not formed in Kendari region but were formed in Baubau region, as well as land units with code names including Wr_Fl_Eut (land unit 31), Wr_Rs_Eut (land unit 33), Wr_Sl_Eut (land unit 35) and Wr_St_Eut (land unit 37) each formed in Kendari region but were not formed in Baubau region. This is due to the intersect process that usually occurs in overlay analysis and is typically influenced by the characteristics of the input data. In this study, the input data referred to is as shown in Table 2 and Figure 2. Further explanation of Table 8, the results of the study indicate that the UHI area in each land unit formed in the two regions shows varying areas.

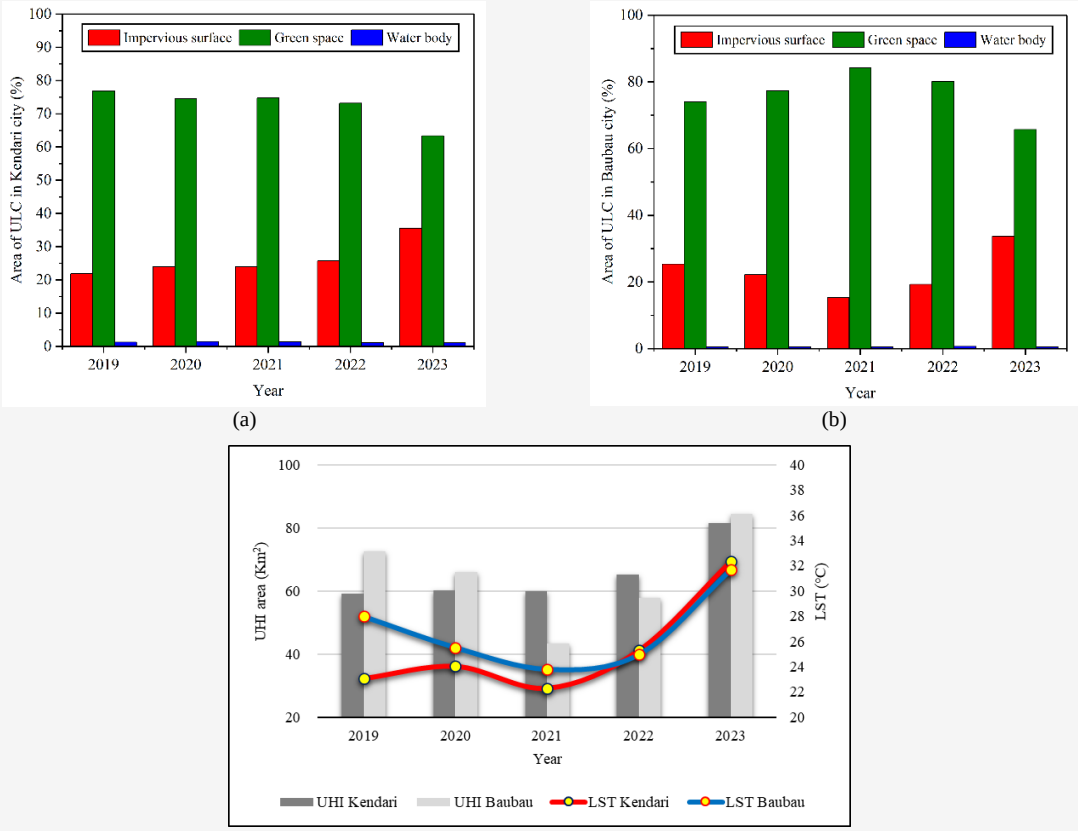

Figure 5: Area of ULC and UHI area in the research sites: (a) Area of ULC in Kendari region; (b) Area of ULC in Baubau region; (c) UHI area in the regions of Kendari and Baubau

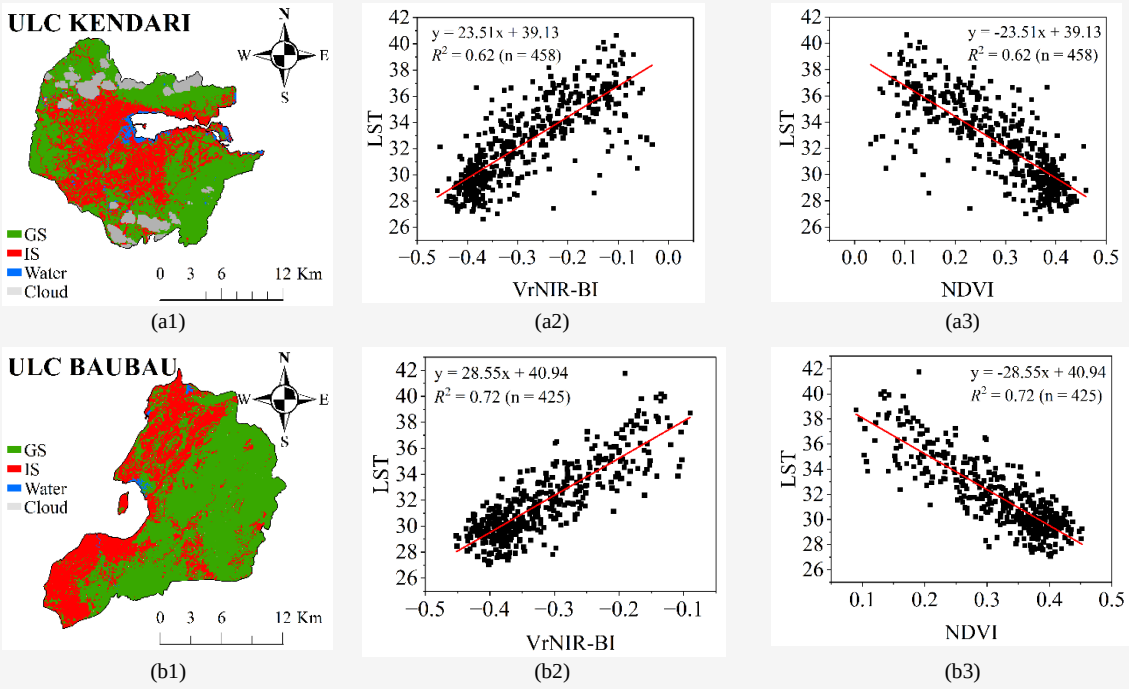

Figure 6: Correlation between LST and indices on urban landscape composition: (a1) – (a3) correlation in the Kendari city and (b1) – (b3) correlation in the Baubau city

Table 8: Land unit area in Km^2 based on UHI area

Land unit	Name code	Area of UHI in Km^2		Land unit	Name code	Area of UHI in Km^2	
		Kendari region	Baubau region			Kendari region	Baubau region
1	Gs_Fl_Dys	0.23126	4.82794	21	Is_Rs_Hap	2.48597	1.44352
2	Gs_Fl_Eut	2.98835	3.08830	22	Is_Sl_Dys	0.86674	7.43474
3	Gs_Fl_Hap	11.34093	7.27607	23	Is_Sl_Eut	0.53635	1.70950
4	Gs_Rs_Dys	0.40777	3.80633	24	Is_Sl_Hap	9.71155	3.91438
5	Gs_Rs_Eut	0.02634	1.11247	25	Is_St_Dys	0.25668	2.78914
6	Gs_Rs_Hap	1.17817	1.55845	26	Is_St_Eut	0.01244	0.29873
7	Gs_Sl_Dys	0.35876	4.83018	27	Is_St_Hap	0.28938	0.44071
8	Gs_Sl_Eut	0.16658	1.87285	28	Is_Vs_Dys	0.00527	0.10877
9	Gs_Sl_Hap	4.09768	2.93402	29	Is_Vs_Eut	-	0.01007
10	Gs_St_Dys	0.20435	2.74903	30	Is_Vs_Hap	0.00477	0.03299
11	Gs_St_Eut	0.00713	0.51699	31	Wr_Fl_Eut	0.06790	-
12	Gs_St_Hap	0.14507	1.08815	32	Wr_Fl_Hap	0.19404	0.02813
13	Gs_Vs_Dys	0.00512	0.21788	33	Wr_Rs_Eut	0.00095	-
14	Gs_Vs_Eut	0.00022	0.05699	34	Wr_Rs_Hap	0.00746	0.01113
15	Gs_Vs_Hap	0.00134	0.27256	35	Wr_Sl_Eut	0.00765	-
16	Is_Fl_Dys	1.01555	7.71401	36	Wr_Sl_Hap	0.03626	0.02118
17	Is_Fl_Eut	10.58645	3.25227	37	Wr_St_Eut	0.00077	-
18	Is_Fl_Hap	33.43858	13.54802	38	Wr_St_Hap	0.00003	0.00522
19	Is_Rs_Dys	0.70251	4.42710	39	Wr_Vs_Hap	-	0.00230
20	Is_Rs_Eut	0.08450	0.91940				

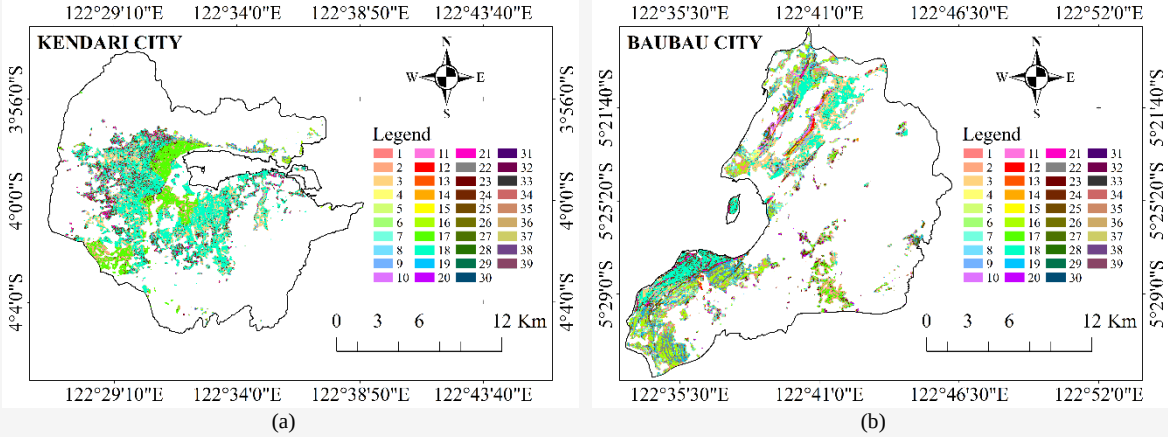

(a) (b)

Figure 7: Spatial distribution of UHI areas on land units: (a) region of Kendari; (b) region of Baubau

In terms of spatial distribution, the largest UHI area in both regions are in the land unit with the code name Is_Fl_Hap or referred to as land unit 18 shown in Figure 7 with a UHI area of 33.43 Km² and 13.55 Km² for regions of Kendari and Baubau respectively and in more detail shown in Figure 8. The characteristics of land unit 18 are classified with a description as area of impervious surface with a relatively flat terrain slope and hapludalfs soil type. This finding is in line with most previous studies, especially in impervious surface area that often became thermal fields in urban environments such as LST concentrations and UHI areas [4][30] and [27]. However, the characteristics of terrain slopes and soil types still require more detailed research in the future, although several previous studies have revealed a relationship with surface temperature and UHI [18][40] and [41]. Nevertheless, in terms of the slope of the terrain we found the tendency of urban infrastructure development in both regions seems to prefer areas that are relatively flat, as a result the formation of UHI in these areas is likely to be accelerated compared to areas with other terrain slopes. Thus, these findings can provide additional new insights in future UHI studies, some of which may be related to the dynamics of urban infrastructure development, detailed landforms and the ratio of low albedo material in land units.

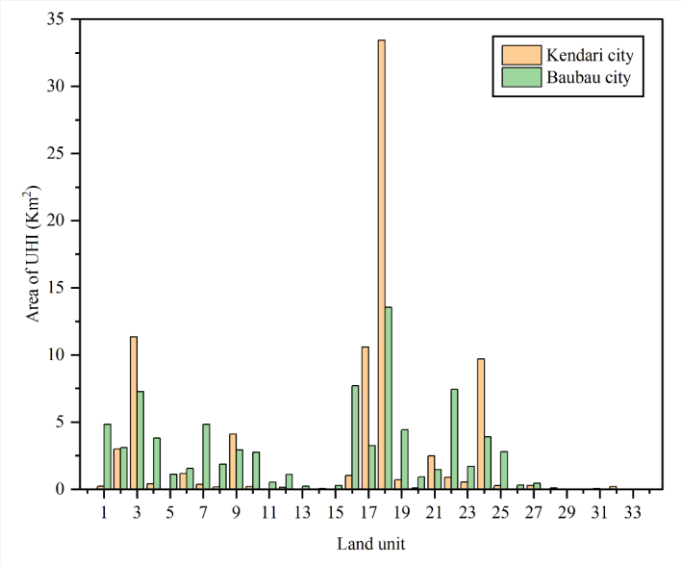

Figure 8: The area of UHI on various land unit in the regions of Kendari and Baubau

Information on UHI variations in land unit areas in this study can generally help stakeholders in both urban areas of Kendari and Baubau in identifying the impacts of urbanization, providing valuable insights for regional development strategy planning and the rate of infrastructure development in urban areas.

5. Conclusion

Based on the analysis results, the surface temperature in the urban thermal environment in both regions is significantly affected by the existing seasonal variations. LST concentrations in both regions are lower in March-June, which are the peak months of the rainy season, then increases to be warmer by around 1.5℃ to 4.9℃ at the peak of the dry season between August-November. In addition, the composition of the urban landscape and global temperature conditions, especially due to the ENSO phenomenon, also influence the variation in LST values in the two regions. The changes in LST that occurred in Kendari and Baubau cities continued to increase in the 2021-2023 period. Significant LST changes occurred in 2022-2023 where the LST change in the Kendari region was +0.3℃ greater than the LST change of +6.7℃ that occurred in the region of Baubau. In 2023 was the warmest year in both cities, it has not been experienced before. This year the summer was very warm occurred in October-November, the highest LST in the two regions reached 41.9℃ and 43.2℃ respectively even the lowest LST had matched the average LST value of other years. Overall, the LST results during the observation period can be used as a basis for monitoring microclimate conditions in both study areas.

In addition to providing valuable insights into microclimate trends in urban thermal environments, LST data is also valuable for assessing the criticality of an environment. For urban planners, variations in LST values can be a reference in planning environmentally friendly, resilient and sustainable cities.

The characteristics of the UHI derived from LST based on Landsat 8/9 imagery in both areas show varying distributions during the observation period. The formation of UHI in both cities are mainly influenced by variations in the average LST concentration and the composition of the urban landscape, typically those categorized as an area of impervious surface. This landscape category shows a positive relationship to LST concentration in both areas. On average, the percentage change in the impervious surface area that occurred in Kendari city during the 2019-2023 period was 26.23%, 3.06% greater than the change that occurred in Baubau city. The area that typically characterizes as an urban area is the center of massive UHI formation in both regions. Spatially, the UHI area in Kendari city appears to be clustered, this is different from Baubau city which appears to be randomly distributed. The dynamics of UHI change in Kendari city tends to moved towards the western region and are more massive to the southern region. Meanwhile, the UHI area in Baubau city is still relatively in the downtown area, but several areas in the northern region of Baubau are beginning to show substantial UHI concentration. The UHI area in both regions continues to expand throughout 2021-2023.

The largest UHI area in the entire study area occurred in 2023. The percentage of UHI area this year reached 30.38% and 29.12% in the Kendari and Baubau regions, respectively. Furthermore, in terms of spatial distribution of land unit characteristics, Land units classified as area of impervious surface with relatively flat terrain slopes and hapludalfs soil types are land units with the largest UHI formation. The formation of UHI areas in these land units is 33.43 km2 and 13.55 km2 in the Kendari and Baubau regions, respectively. The dynamics of UHI changes throughout the study area tend to show the same pattern as the impervious surface area. Interestingly, based on the area of UHI in each land unit, several green space areas and water bodies that are specifically negatively correlated with LST are also part of the UHI area. This finding still requires further investigation. Findings related to the trend of expansion and direction of UHI movement can be used as a reference for stakeholders, especially in making decisions related to disaster mitigation efforts due to increasing surface temperatures, including the negative impacts of UHI caused in each land unit. This study has several limitations such as the UHI discussed only shows the UHI at day time and the scale presented is only at the level of the municipal administrative area. Further research is recommended to explore the formation between daytime and nighttime UHI and observe the formation of UHI at a more detailed administrative level such as sub-districts to small areas.

Acknowledgements

This research is supported by the Directorate of Research, Technology and Community Service, Directorate General of Higher Education, Research, and Technology, Ministry of Education, Culture, Research, and Technology, grant number 049/E5/PG.02.00.PL/2024. The authors would like to thank all parties who have supported and assisted in the implementation of the program and also to the reviewers of this article.

References

[1] Mardiansjah, F. H., Rahayu, P. and Rukmana, D., (2021). New Patterns of Urbanization in Indonesia: Emergence of Non-statutory Towns and New Extended Urban Regions. *Environment and Urbanization ASIA*, Vol. 12. https://doi.org/10.1177/0975425321990384.

[2] Guo, L., Liu, R., Men, C., Wang, Q., Miao, Y. and Zhang, Y., (2019). Quantifying and Simulating Landscape Composition and Pattern Impacts on Land Surface Temperature: A Decadal Study of the Rapidly Urbanizing City of Beijing, China. *Science of The Total Environment*, Vol. 654. https://doi.org/10.1016/j.scitotenv.2018.11.108.

[3] Zeng, Q., Xie, Y. and Liu, K., (2019). Assessment of the Patterns of Urban Land Covers and Impervious Surface Areas: A Case Study of Shenzhen, China. *Physics and Chemistry of the Earth*, Vol. 110. https://doi.org/10.1016/j.pce.2019.04.002.

[4] Estoque, R. C., Murayama, Y. and Myint, S. W., (2017). Effects of Landscape Composition and Pattern on Land Surface Temperature: An Urban Heat Island Study in the Megacities of Southeast Asia. *Science of The Total Environment*, Vol. 577. https://doi.org/10.1016/j.scitotenv.2016.10.195.

[5] Voogt, J. A. and Oke, T. R., (2003). Thermal Remote Sensing of Urban Climates. *Remote Sensing of Environment*, Vol. 86. https://doi.org/10.1016/S0034-4257(03)00079-8.

[6] Hibbard, K. A., Hoffman, F. M., Huntzinger, D. and West, T. O., (2017). Changes in Land Cover and Terrestrial Biogeochemistry. *Climate Science Special Report: Fourth National Climate Assessment*, 1st ed., Vol. 1, D. J. Wuebbles, D. W. Fahey, K. A. Hibbard, D. J. Dokken, B. C. Stewart, T. K. Maycock, Ed. Washington, DC: U.S. Global Change Research Program, 2017, 277–302.

[7] El-Hattab, M., Amany, S. M. and Lamia, G. E., (2018). Monitoring and Assessment of Urban Heat Islands over the Southern Region of Cairo Governorate, Egypt. *The Egyptian Journal of Remote Sensing and Space Science*, Vol. 21. https://doi.org/10.1016/j.ejrs.2017.08.008.

[8] Intergovernmental Panel on Climate Change (IPCC), (2023). *Climate Change 2021 – The Physical Science Basis: Working Group I Contribution to the Sixth Assessment Report of the Intergovernmental Panel on Climate Change*, Cambridge: Cambridge University Press, 2023. [E-book] Available: Cambridge Core.

[9] Intergovernmental Panel on Climate Change (IPCC), (2023). *Climate Change 2022 – Impacts, Adaptation and Vulnerability: Working Group II Contribution to the Sixth Assessment Report of the Intergovernmental Panel on Climate Change*, Cambridge: Cambridge University Press, 2023. [E-book] Available: Cambridge Core.

[10] Syafitri, R. A. W. D., Pamungkas, A. and Santoso, E. B., (2020). The Impact of Urban Configuration to the UHI in East Surabaya. *Fostering Innovation Projects for Business Growth: Proceedings of the 6th International*

Seminar on Science and Technology, ISST 2020, Surabaya, Indonesia, July 25, 2020, Nadlifatin R., Bhawika G. W., Eds. Institut Teknologi Sepuluh Nopember, 2020. 470–477.

[11] Bonifacio-Bautista, M., Ballinas, M., Jazcilevich, A. and Barradas, V. L., (2022). Estimation of Anthropogenic Heat Release in Mexico City. *Urban Climate*, Vol. 43. https://doi.org/10.1016/j.uclim.2022.101158.

[12] Ibrahim, M. and Abu-Mallouh, H., (2018). Estimate Land Surface Temperature in Relation to Land Use Types and Geological Formations Using Spectral Remote Sensing Data in Northeast Jordan. *Open Journal of Geology*, Vol. 8. https://doi.org/10.4236/ojg.2018.82011.

[13] Tang, J., Lan, X., Lian, Y., Zhao, F. and Li, T., (2022). Estimation of Urban–Rural Land Surface Temperature Difference at Different Elevations in the Qinling–Daba Mountains Using MODIS and the Random Forest Model. *International Journal of Environmental Research and Public Health*, Vol. 19. https://doi.org/10.3390/ijerph191811442.

[14] Jagtap, A., Shedge, D., and Mane, P. (2024). Exploring the Effects of Land Use/Land Cover (LULC) Modifications and Land Surface Temperature (LST) in Pune, Maharashtra with Anticipated LULC for 2030. *International Journal of Geoinformatics*, Vol. 20(2), 42–63. https://doi.org/10.52939/ijg.v20i2.3065.

[15] Wang, S., Wang, Z., Zhang, Y. and Fan, Y., (2022). Characteristics of Urban Heat Island in China and its Influences on Building Energy Consumption. *Applied Sciences*, Vol. 12. https://doi.org/10.3390/app12157678.

[16] Zhang, M., Tan, S., Liang, J., Zhang, C. and Chen, E., (2024). Predicting the Impacts of Urban Development on Urban Thermal Environment Using Machine Learning Algorithms in Nanjing, China. *Journal of Environmental Management*, Vol. 356. https://doi.org/10.1016/j.jenvman.2024.120560

[17] Li, X., Stringer, L. C. and Dallimer, M., (2022). The Impacts of Urbanisation and Climate Change on the Urban Thermal Environment in Africa. *Climate*, Vol. 10. https://doi.org/10.3390/cli10110164.

[18] Liu, X., Ming, Y., Liu, Y., Yue, W. and Han, G., (2022). Influences of Landform and Urban form Factors on Urban Heat Island: Comparative Case Study between Chengdu and Chongqing. *Science of The Total Environment*, Vol. 820. https://doi.org/10.1016/j.scitotenv.2022.153395.

[19] Sayler, K. and Zanter, K., (2023). Landsat 8-9 Collection 2 Level 2 Science Product Guide. *Department of the Interior United States Geological Survey*. [Online]. Available: https://www.usgs.gov/media/files/landsat-8-9-collection-2-level-2-science-product-guide. [Accessed Aug. 10, 2024].

[20] Weng, Q., Lu, D. and Schubring, J., (2004). Estimation of Land Surface Temperature–Vegetation Abundance Relationship for Urban Heat Island Studies. *Remote Sensing of Environment*, Vol. 89. https://doi.org/10.1016/j.rse.2003.11.005.

[21] Estoque, R. C. and Murayama, Y., (2015). Classification and Change Detection of Built-Up Lands from Landsat-7 ETM+ and Landsat-8 OLI/TIRS Imageries: A Comparative Assessment of Various Spectral Indices. *Ecological Indicators*, Vol. 56. https://doi.org/10.1016/j.ecolind.2015.03.037.

[22] Sobrino, J. A., Jiménez-Muñoz, J. C. and Paolini, L., (2004). Land Surface Temperature Retrieval from LANDSAT TM 5. *Remote Sensing of Environment*, Vol. 90. https://doi.org/10.1016/j.rse.2004.02.003.

[23] Sobrino, J. A., Jiménez-Muñoz, J. C., Sòria, G., Romaguera, M., Guanter, L., Moreno, J., Plaza, A. and Martínez, P., (2008). Land Surface Emissivity Retrieval from Different VNIR and TIR Sensors. *IEEE Transactions on Geoscience and Remote Sensing*, Vol. 46. https://doi.org/10.1109/TGRS.2007.904834.

[24] Hou, H. and Estoque, R. C., (2020). Detecting Cooling Effect of Landscape from Composition and Configuration: An Urban Heat Island Study on Hangzhou. *Urban Forestry & Urban Greening*, Vol. 53. https://doi.org/10.1016/j.ufug.2020.126719.

[25] Sameh, S., Zarzoura, F., and El-Mewafi, M. (2022). Automated Mapping of Urban Heat Island to Predict Land Surface Temperature and Land use/cover Change Using Machine Learning Algorithms: Mansoura City. *International Journal of Geoinformatics*, Vol. 8(6), 47–67. https://doi.org/10.52939/ijg.v18i6.2461.

[26] Zhang, X., Estoque, R. C., Murayama, Y. and Ranagalage, M., (2021). Capturing Urban Heat Island Formation in a Subtropical City of China Based on Landsat Images: Implications for Sustainable Urban Development. *Environmental Monitoring and Assessment*, Vol. 193. https://doi.org/10.1007/s10661-021-08890-w.

[27] Thammaboribal, P., (2024). Investigating Land Surface Temperature Variation and Land Use Land Cover Changes in Pathumthani, Thailand (1997-2023) using Landsat Satellite Imagery: A Comprehensive Analysis of LST and Urban Hot Spots (UHS). *International Journal of Geoinformatics*, Vol. 20(2), 27–41. https://doi.org/10.52939/ijg.v20i2.3063.

[28] Ma, Y., Kuang, Y. and Huang, N., (2010). Coupling Urbanization Analyses for Studying Urban Thermal Environment and Its Interplay with Biophysical Parameters Based on TM/ETM+ Imagery. *International Journal of Applied Earth Observation and Geoinformation*, Vol. 12, 110-118. https://doi.org/10.1016/j.jag.2009.12.002.

[29] Simwanda, M., Spatial Analysis of Surface Urban Heat Islands in Four Rapidly Growing African Cities Ranagalage, M., Estoque, R. C. and Murayama, Y., (2019). *Remote Sensing*, Vol. 11. https://doi.org/10.3390/rs11141645.

[30] Siswanto, S., Nuryanto, D. E., Ferdiansyah, M. R., Prastiwi, A. D., Dewi, O. C., Gamal, A. and Dimyati, M., (2023). Spatio-Temporal Characteristics of Urban Heat Island of Jakarta Metropolitan. *Remote Sensing Applications: Society and Environment*, Vol. 32. https://doi.org/10.1016/j.rsase.2023.101062.

[31] Handayani, H. H., Estoque, R. C. and Murayama, Y., (2018). Estimation of Built-Up and Green Volume using Geospatial Techniques: A Case Study of Surabaya, Indonesia. *Sustainable Cities and Society*, Vol. 37. https://doi.org/10.1016/j.scs.2017.10.017.

[32] World Meteorological Organization (WMO), (2024). *State of the Global Climate 2023,* Geneva: WMO, 2023. [E-book] Available: WMO e-library.

[33] Perkins-Kirkpatrick, S., Barriopedro, D., Jha, R., Wang, L., Mondal, A., Libonati, R. and Kornhuber, K., (2024). Extreme Terrestrial Heat in 2023. *Nature Reviews Earth & Environment*, Vol. 5. https://doi.org/10.1038/s43017-024-00536-y.

[34] Prasetyaningtyas, K., (2023). Analisis Dinamika Atmosfer Dasarian II November 2023 [Analysis of Atmospheric Dynamics for the Second Ten-Day Period of November 2023]. *Badan Meteorologi, Klimatologi, dan Geofisika [The Agency for Meteorology, Climatology and Geophysics]*. [Online]. Available: https://www.bmkg.go.id/berita/?p=analisis-dinamika-atmosfer-dasarian-ii-november-2023&lang=ID&tag=dinamika-atmosfer. [Accessed Sep. 24, 2024].

[35] Prasetyaningtyas, K., (2023). Analisis Dinamika Atmosfer Dasarian III Oktober 2023 [Analysis of Atmospheric Dynamics for the Third Ten-Day Period of November 2023]. *Badan Meteorologi, Klimatologi, dan Geofisika [The Agency for Meteorology, Climatology and Geophysics]*. [Online]. Available: https://www.bmkg.go.id/berita/?p=analisis-dinamika-atmosfer-dasarian-iii-oktober-2023&lang=ID&tag=dinamika-atmosfer. [Accessed Sep. 30, 2024].

[36] Jaelani, L. M. and Handayani, C. A., (2022). Spatio-temporal Analysis of Land Surface Temperature Changes in Java Island from Aqua and Terra MODIS Satellite Imageries Using Google Earth Engine. *International Journal of Geoinformatics*, Vol. 18(5). 1–12. https://doi.org/10.52939/ijg.v18i5.2365.

[37] Buyantuyev, A. and Wu, J., (2010). Urban Heat Islands and Landscape Heterogeneity: Linking Spatiotemporal Variations in Surface Temperatures to Land-Cover and Socioeconomic Patterns. *Landscape Ecology*, Vol. 25. https://doi.org/10.1007/s10980-009-9402-4.

[38] Senanayake, I. P., Welivitiya, W. D. D. P. and Nadeeka, P. M., (2013). Remote Sensing Based Analysis of Urban Heat Islands with Vegetation Cover in Colombo City, Sri Lanka using Landsat-7 ETM+ Data. *Urban Climate*, Vol. 5. https://doi.org/10.1016/j.uclim.2013.07.004.

[39] Khan, A., Chatterjee, S. and Weng, Y., (2021). UHI Drivers and Mapping the Urban Thermal Environment. *Urban Heat Island Modeling for Tropical Climates*, 1st ed., A. Khan, S. Chatterjee, Y. Weng, Ed. Amsterdam: Elsevier, 2021, 69-115.

[40] Sianturi, R. S., Perdana, A. P. and Ramdani, F., (2024). Monitoring Land Surface Temperature Trends in Indonesia. *IOP Conference Series: Earth and Environmental Science*, Vol. 1353. https://doi.org/10.1088/1755-1315/1353/1/012036.

[41] Liao, S., Cai, H., Tian, P., Zhang, B. and Li, Y., (2022). Combined Impacts of the Abnormal and Urban Heat Island Effect in Guiyang, a Typical Karst Mountain City in China. *Urban Climate*, Vol. 41. https://doi.org/10.1016/j.uclim.2021.101014.